European Journal of Medicinal Chemistry 46 (2011) 2243–2251

Contents lists available at ScienceDirect

European Journal of Medicinal Chemistry

journal homepage: http://www.elsevier.com/locate/ejmech

Original article

Antidiabetic activity of some pentacyclic acid triterpenoids, role of PTP–1B: *In vitro*, *in silico*, and *in vivo* approaches☆

Juan José Ramírez-Espinosa [a], Maria Yolanda Rios [b], Sugey López-Martínez [b], Fabian López-Vallejo [c], José L. Medina-Franco [c], Paolo Paoli [d], Guido Camici [d], Gabriel Navarrete-Vázquez [a], Rolffy Ortiz-Andrade [e], Samuel Estrada-Soto [a,*]

[a] Facultad de Farmacia, Universidad Autónoma del Estado de Morelos, Avenida Universidad 1001, Col. Chamilpa, Cuernavaca, Morelos 62209, Mexico
[b] Centro de Investigaciones Químicas, Universidad Autónoma del Estado de Morelos, Avenida Universidad 1001, Col. Chamilpa, Cuernavaca, Morelos 62209, Mexico
[c] Torrey Pines Institute for Molecular Studies, Port St. Lucie, FL 34987, USA
[d] Dipartimento di Scienze Biochimiche, Universitá degli Studi di Firenze, Viale Morgani 50, 50134 Firenze, Italy
[e] Facultad de Química, Universidad Autónoma de Yucatán, Mérida, Calle 421 No. 41 x 26 y 28 Col. Industrial, C.P. 97150 Mérida Yucatán 97150, Mexico

ARTICLE INFO

Article history:
Received 27 October 2010
Received in revised form
28 February 2011
Accepted 1 March 2011
Available online 10 March 2011

Keywords:
Diabetes
Pentacyclic triterpenoids
PTP-1B
Docking
Enzyme inhibition

ABSTRACT

The aim of the current study was to investigate the oral antidiabetic activity of four structurally-related triterpenic acids: ursolic (**RE-01**), oleanolic (**RE-02**), moronic (**RE-03**) and morolic (**RE-04**) acids. STZ-nicotinamide diabetic rats were treated with these triterpenes (50 mg/kg) and the antidiabetic effects in acute experiment were determined. All compounds showed significant antidiabetic activity in comparison with control group ($p < 0.05$). The *in vitro* inhibitory activity of compounds against protein tyrosine phosphatase 1B (PTP–1B) was also evaluated. At 50 μM, the enzymatic activity was almost completely inhibited. All compounds were docked with a crystal structure of PTP–1B. Docking results suggested the potential binding of the triterpenic acids in a binding pocket next to the catalytic site. An extensive hydrogen bond network with the carboxyl group and Van der Waals interactions stabilize the protein-ligand complexes.

1. Introduction

Diabetes mellitus (DM) is a chronic disease that occurs when the pancreas does not produce enough insulin or when the body cannot effectively use it, resulting in hyperglycemia. Over time this condition can cause serious damage to several body systems, in particular the nerves and blood vessels. Type 2 DM, or non insulin dependent diabetes, results from ineffective use of insulin as consequence of excess body weight, physical inactivity, and genetic susceptibility [1]. This disease has been becoming more common because of a lifestyle and diet that promotes obesity; it's particularly prevalent in Hispanic and aging populations [2]. Treatment of diabetes involves lowering blood glucose through different mechanisms, including insulin secretion, glucose absorption, and metabolism [3]. Activation of PPAR-α and PPAR-γ by rosiglitazone [4] or inhibition of dipeptidyl peptidase-4 (DPP-4) by sitagliptin [5] are novel approaches for the treatment of diabetes. Protein tyrosine phosphatase 1B (PTP–1B) has recently shown an important influence over insulin sensitivity since it is implicated in modulating insulin signal transduction becoming a key regulator of insulin-receptor activity and downstream signaling pathways [6]. This is related with a dephosphorylation of active insulin receptor (IR) [7]. Studies carried out with knock-out mice suggest that the lack of PTP–1B enzyme would result in activated insulin receptors, improved sensibility to insulin, and stimulated glucose uptake [8].

The study of medicinal plants has lead to the discovery of new chemical structures for potential development as drugs that act over new or known therapeutic targets. Thus, the *Phoradendron* genus has been used in Mexico since ancient times for the treatment of diabetes, hypertension, among other diseases [9]. Pentacyclic acid triterpenoids and other compounds isolated from *Phoradendron reichenbachianum*, a parasitic herbal of Holm oaks, have shown significant cytotoxic [10] and antiviral activities [11].

In an attempt to find novel antidiabetic drugs from medicinal plants, herein we report *in vivo, in silico*, and *in vitro* studies of a series of structurally-related pentacyclic acid triterpenoids (Fig. 1)

☆ Taken in part from Master in Pharmacy thesis of J.J. Ramírez-Espinosa (Pharmacological Research) and Postdoctoral stay of S. López (Phytochemical investigation).

* Corresponding author. Tel./fax: +52 777 329 7089.
E-mail address: enoch@uaem.mx (S. Estrada-Soto).

0223-5234/$ – see front matter © 2011 Elsevier Masson SAS. All rights reserved.
doi:10.1016/j.ejmech.2011.03.005

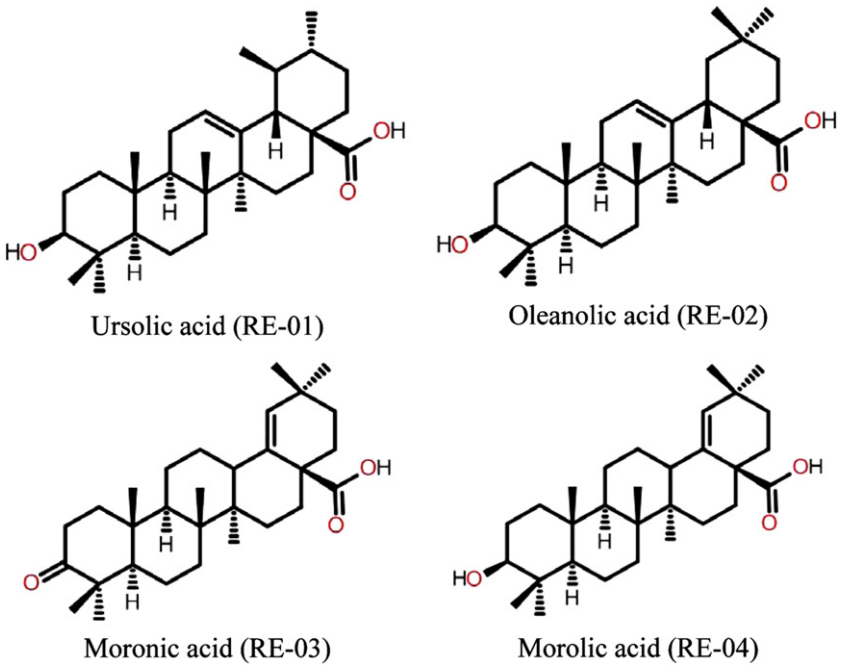

Fig. 1. Compounds evaluated.

using the streptozotocin-nicotinamide induced diabetic rat model. In addition, we report the results of *in vitro* enzymatic and *in silico* experiments and discuss the possible mechanism of action of these metabolites through the inhibition of PTP−1B.

2. Results and discussion

2.1. Chemistry

Ursolic (**RE-01**), oleanolic (**RE-02**), moronic (**RE-03**), and morolic (**RE-04**) acids were purified and characterized from acetone extract of leaves and stems of *Phoradendron reichenbachianum* (AEP*r*) as previously reported in Reference [10].

2.2. In vivo antidiabetic activity

Table 1 shows that i.g. administration of AEP*r* (100 mg/kg) and **RE-01**, **RE-02**, **RE-03** and **RE-04** (50 mg/kg), induced, in general, a significant decrease in plasma glucose concentration in diabetic rats ($p < 0.05$) during acute time periods (7 h) as compared with the control group (vehicle). All compounds showed significant antidiabetic activity, in particular **RE-01** and **RE-03** showed the best activity as compared with the control group ($p < 0.05$). **RE-01** and **RE-03** produced a sustained decrease of blood glucose levels, close to 25%, during all the experiment. The *in vivo* antidiabetic activity of **RE-01** and **RE-02** on streptozotocin-induced diabetic rats has been described in References [12,13]. Also, **RE-02** significantly ($p < 0.05$) improved the glucose tolerance test at the 30 min period with a maximal decline at 10 mg/kg. Compared to vehicle-treated control, **RE-02** lowered the blood glucose levels by 30, 37, and 22%, respectively, for the respective doses [14]. These previous reports are in agreement with our results made on the non insulin-dependent diabetes model. On the other hand, AEP*r* showed the same potency as pure compounds, which suggests a possible additive action of triterpenic acids contained there. Moreover, this is the first report concerning the *in vivo* antidiabetic effect of AEP*r*, **RE-03**, and **RE-04**.

The *in vitro* enzymatic activity of **RE-01** and **RE-02** as antidiabetic agents has been reported; both triterpenic acids induced a significant PTP−1B [15,16] and 11β-HSD1 [17,18] enzymatic inhibition. **RE-02** enhanced the IRβ tyrosine kinase activity and also enhanced the effect of insulin on translocation of glucose transporter 4 in 3T3−L1 adipocytes, a classical insulin-sensitive cell line [19]. Therefore, we decided to determine the *in vitro* enzymatic PTP−1B inhibition of **RE-03** and **RE-04** as structural related analogs of **RE-01** and **RE-02**. We also conducted automated docking studies in order to propose a binding model with PTP−1B.

2.3. In vitro PTP−1B assay

To test the ability of each compound to inhibit PTP−1B, aliquots of stock solutions (dissolved in DMSO to prepare 20 mM) were diluted with the assay buffer, containing 2.5 mM *p*-nitrophenyl phosphate

Table 1
Percentage of variation of blood glucose concentration on streptozotocin-nicotinamide induced diabetic rats treated with AE*Pr* and pentacyclic acid triterpenoids.

Test samples	Dose (mg/Kg)	Percentage of variation of glycemia ± S.E.M. (mg/dL)				
		Zero hour	First hour	Third hour	Fifth hour	Seventh hour
Vehicle	–	0 ± 0.0	9.1 ± 10.98	−1.71 ± 5.11	−0.51 ± 5.11	−5.67 ± 6.09
Glibenclamide	5	0 ± 0.0	−20.43 ± 8.17*	−36.34 ± 7.55*	−37.48 ± 7.16*	−43.64 ± 9.9*
AE*Pr*	100	0 ± 0.0	−20.3 ± 6.17*	−17.55 ± 3.15*	−26.42 ± 10.87*	−28.53 ± 6.62*
RE-01	50	0 ± 0.0	−13.46 ± 7.7*	−24.45 ± 10.9*	−25.66 ± 9.78*	−38.01 ± 5.0*
RE-02	50	0 ± 0.0	−26.92 ± 5.7*	−14.1 ± 6.78*	−23.2 ± 9.9*	−21.92 ± 8.9*
RE-03	50	0 ± 0.0	−17.3 ± 5.6*	−26.3 ± 5.9*	−15.3 ± 3.6*	−29.2 ± 4.0*
RE-04	50	0 ± 0.0	−1.54 ± 5.02*	−15.23 ± 3.84*	−8.77 ± 4.86	−39.18 ± 2.72*

* Values represent the mean ± S.E.M. ($n = 6$). $p < 0.05$ compared with control group. The negative value (−) indicates decrease in glycemia.

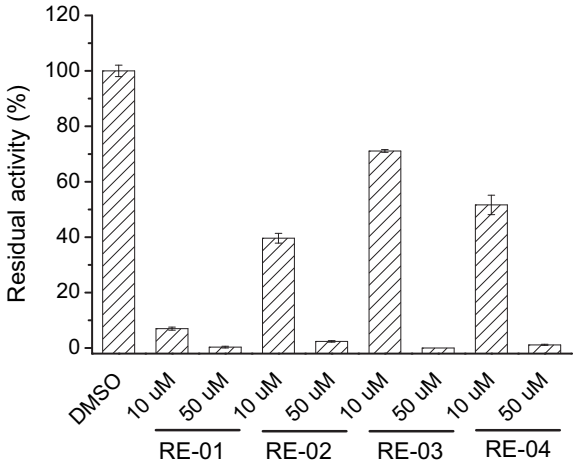

Fig. 2. Assay of inhibition activity of ursolic (**RE-01**), oleanolic (**RE-02**), moronic (**RE-03**), and morolic (**RE-04**) acids at 10 and 50 μM against PTP. All assays were performed in 0.075 M β,β-dimethylglutarate buffer pH 7.0, containing 1 mM EDTA and 1 mM dithiothreitol. The final concentration of the substrate (*p*NPP) in each assay was 2.5 mM. All experiments were performed in triplicate. The data reported represent the mean ± S.E.M.

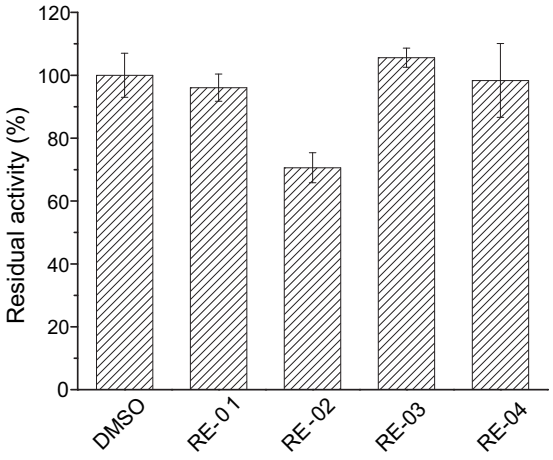

Fig. 4. Inhibition reversibility assay. Aliquots of PTP were incubated in the presence of a fixed concentration of each compound for 1 h at 37 °C (**RE-01**, 10 μM; **RE-02**, 25 μM; **RE-03**, 35 μM; **RE-04**, 25 μM). Then, the enzyme was diluted 400-fold with the assay solution to measure the residual activity (37 °C, 10 mM *p*NPP). Control experiments were carried out adding DMSO. All tests were performed in triplicate. The data represent the mean ± S.E.M.

(*p*NPP), to obtain two different inhibitor concentrations. Samples were incubated at 37 °C, and the reactions were initiated by adding an appropriate enzyme aliquot. Fig. 2 shows the preliminary results. This figure clearly shows that all compounds induced a significant enzyme inhibition at both evaluated concentrations (10 and 50 μM), and the inhibition effects were more pronounced at the highest concentration.

In order to determine the IC_{50} value of each compound, the enzyme activity was measured at a fixed substrate concentration (corresponding to the K_m) and varying inhibitor concentrations. IC_{50} values were calculated by fitting experimental data in the following equation, using a non-nonlinear fitting program (FigSys, Biosoft, UK):

$$y = \frac{Max - Min}{1 + \left(\frac{x}{IC_{50}}\right)^{slope}} + Min$$

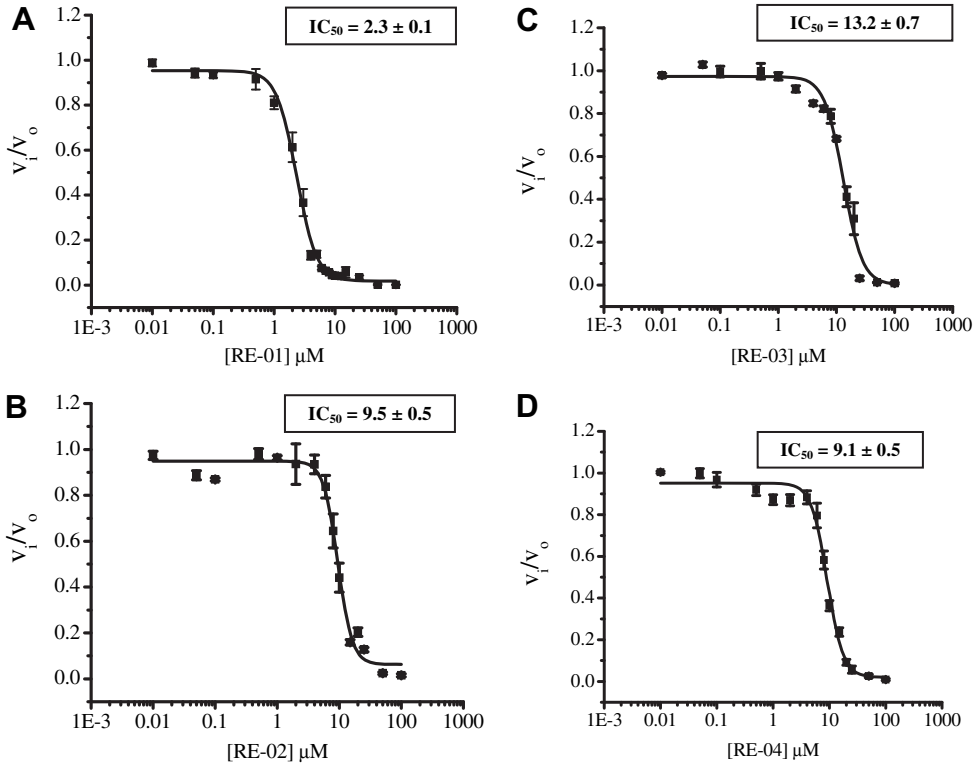

Fig. 3. A–D: IC_{50} determination. The IC_{50} value for compounds **RE-01** (A), **RE-02** (B), **RE-03** (C) and **RE-04** (D) were determined by plotting the data relative to the residual activity of the PTP against the inhibitor concentration. 15–18 different inhibitor concentrations were used for each inhibitor. All assays were performed in quadruplicate. Data represent the mean ± S.E.M.

Table 2
The IC_{50} values determined for different PTPases. For each inhibitor, between 15 and 18 different inhibitor concentrations were used. All tests were performed in triplicate. The data represent the mean ± S.E.M.

Compound	**RE−01**	**RE−02**	**RE−03**	**RE−04**
Enzyme	IC_{50} (μM)			
PTP-1B	2.3 ± 0.1	9.5 ± 0.5	13.2 ± 0.7	9.1 ± 0.5
IF1	7.2 ± 0.2	21.2 ± 0.5	20.6 ± 0.6	13.4 ± 0.4
IF2	11.1 ± 0.3	22.9 ± 0.9	27.4 ± 1.5	30.6 ± 0.7
LTP1	20 ± 0.7	44.8 ± 1.7	51.2 ± 0.9	52.0 ± 0.3
LAR	3.8 ± 0.1	11.8 ± 1.0	45.6 ± 3.0	35.9 ± 8.3

where $y = v_i/v_o$ is the ratio between the measured activity in the presence of the inhibitor (v_i) and the activity of the control without the inhibitor (v_o). x is the inhibitor concentration.

All compounds induced a PTP−1B enzymatic inhibition in a concentration-dependent manner (Fig. 3A−D). Moreover, **RE-01** and **RE-04** were the most potent inhibitors. **RE-01** and **RE-02** acids have been reported as inhibitors of PTP−1B with IC_{50} values of 3.28 and 3.02 μM, respectively [15,16]. These results are in agreement with our previous observations (Fig. 3A−D). Yet for **RE-03** and **RE-04** acids, there are no reports concerning their PTP−1B inhibitory properties. Also, the selectivity and type of inhibition for these compounds have not been reported. Therefore, the dilution method was used to determine the ability of each compound to dissociate from PTP−1B after binding. The enzyme was incubated for 1 h at 37 °C in the presence of each inhibitor. Then aliquots of enzyme mixture was withdrawn and diluted with the assay buffer to determine the residual activity. Fig. 4 summarizes the results indicating that the recovery of enzyme activity is almost complete in all cases, with the exception of **RE-02**, suggesting that most compounds behave as reversible inhibitors.

We also determined the selectivity of each inhibitor towards other none structurally related PTPases, such as the IF1, IF2 isoenzymes of human LMW-PTP, the yeast LMW-PTP (LTP1) and human LAR. The selectivity was measured at the corresponding experimental IC_{50} value of each compound. Results are summarized in Table 2. All IC_{50} values for other PTPases were higher than the corresponding IC_{50} value for PTP−1B. These results indicate that all compounds are selective towards PTP−1B with respect to the other PTPases tested.

To determine the inhibition mechanism of each compound, we studied the effects of increasing inhibitors concentration on main kinetics parameters, K_m and V_{max} (Figs. 5−8). We deduced from the experimental results that the inhibition mechanism of compounds **RE-01**, **RE-02** and **RE-03** (Figs. 5−7) can be referred to a linear mixed-type inhibition model (Scheme 1), suggesting a possible binding in a different cavity from the catalytic site. This was further supported with molecular docking results discussed later. In contrast, the inhibition mechanism of **RE-04** (Fig. 8) can be referred to a simple linear non-competitive inhibition model. The *Ki* values for all compounds were calculated using the appropriate equations and are presented in Table 3.

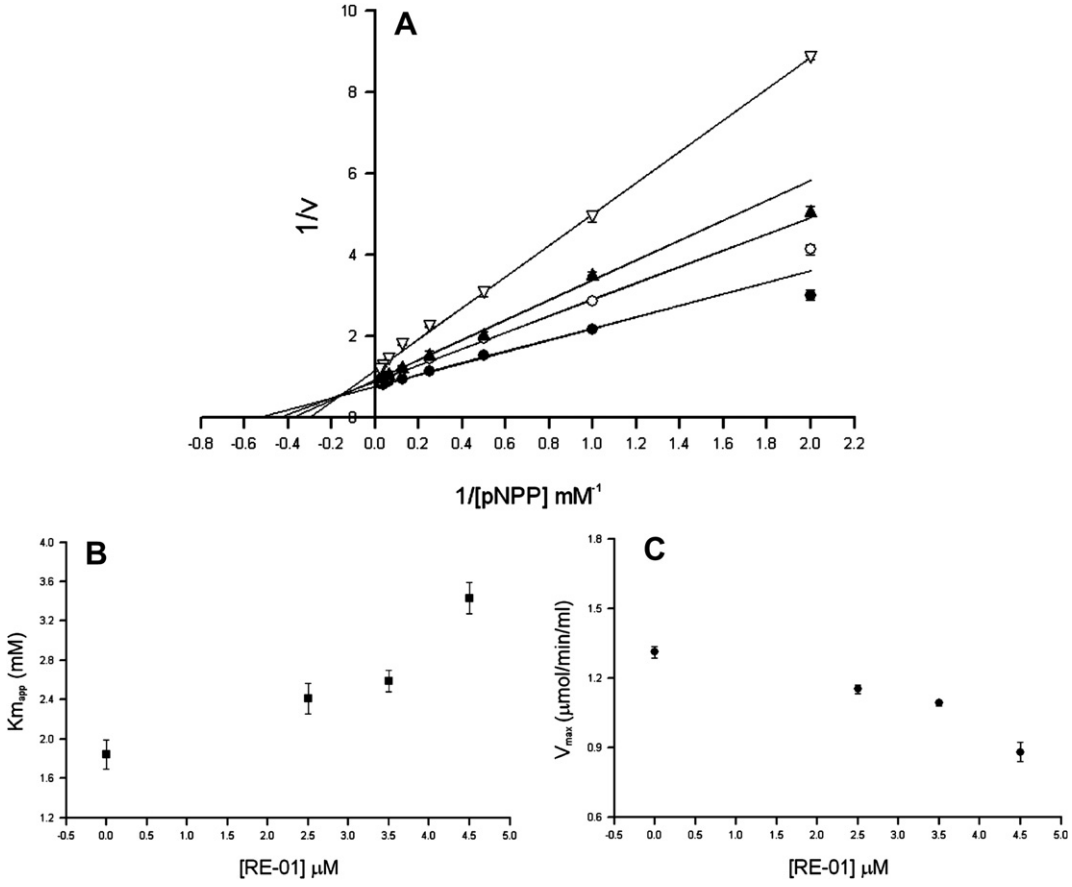

Fig. 5. Double reciprocal plot of **RE-01** (1/*v* versus 1/[*S*]) (A), the inhibitor concentrations were: 0 μM ●; 2.5 μM ○; 3.5 μM ▲; 4.5 μM ▽. Dependence of main kinetic parameters K_m (B) and V_{max} (C) from the concentration of **RE-01**, the inhibitor concentrations were: 0, 2.5, 3.5 and 4.5 μM. All assays were performed by triplicate. The data reported in the graph, represent the means (A) or values (B and C) ± S.E.M.

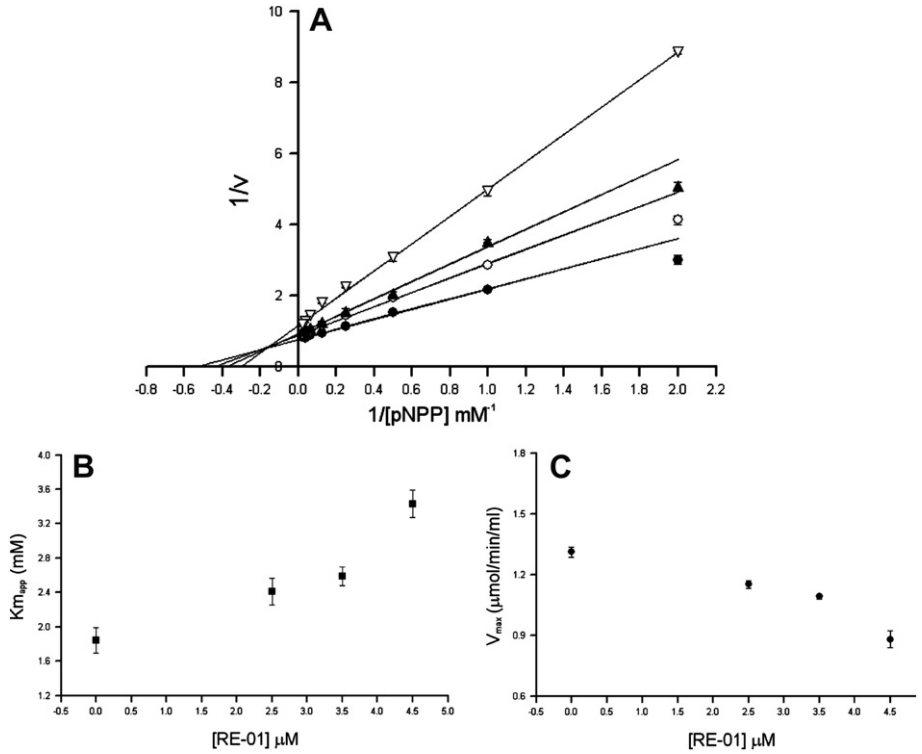

Fig. 6. Compound **RE-02**. Double reciprocal plot (1/v versus 1/[S]) (A), the inhibitor concentrations were: 0 μM ■; 6.5 μM ○; 10.5 μM ▲; 14.5 μM ▽. Dependence of main kinetic parameters K_m (B) and V_{max} (C) from the concentration of **RE-02**, the concentrations of inhibitor used were: 0, 6.5, 10.5 and 14.5 μM. All assays were performed by triplicate. The data reported in the graph, represent the means (A) or values (B and C) ± S.E.M.

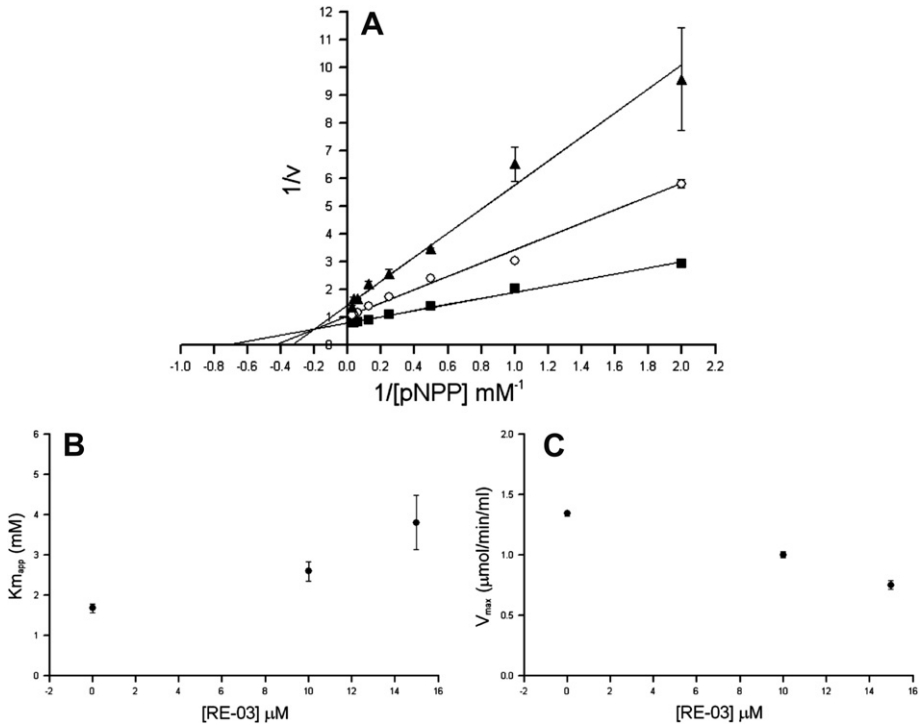

Fig. 7. Compound **RE-03**. Double reciprocal plot (1/*v* versus 1/[*S*]) (A), the concentrations of inhibitor used were: 0 μM ■; 10 μM ○; 15 μM ▲. Dependence of main kinetic parameters K_m (B) and V_{max} (C) from the concentration of compound **RE-03**, the concentrations of inhibitor used were: 0, 10 and 15 μM. All assays were performed by triplicate. The data reported in the graph, represent the means (A) or values (B and C) ± S.E.M.

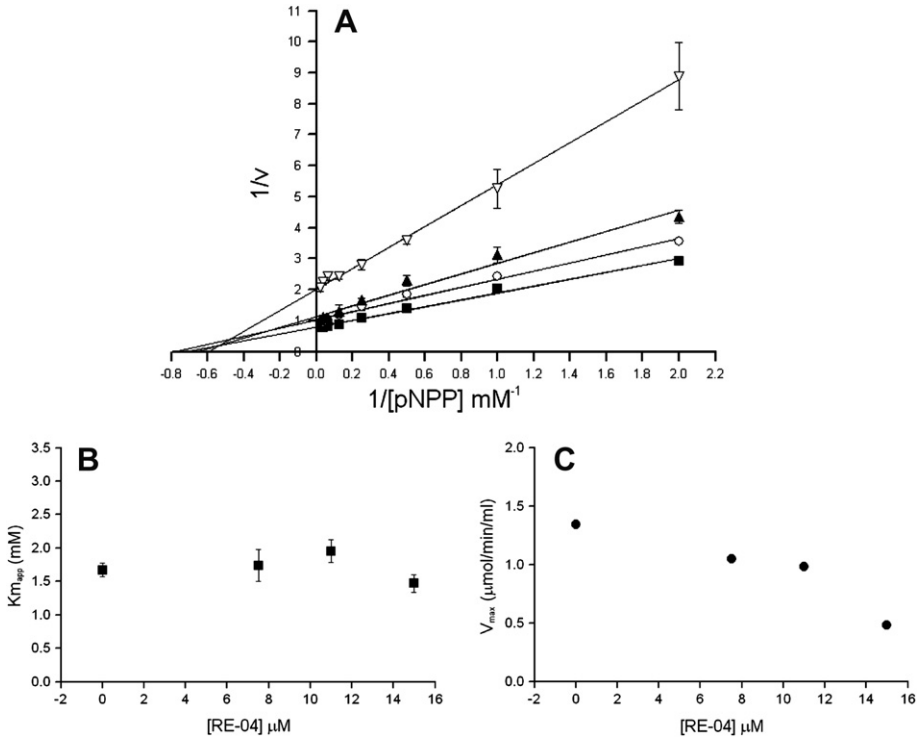

Fig. 8. Double reciprocal plot of **RE-04** (1/v versus 1/[S]) (A), the concentrations of inhibitor used were: 0 µM ■; 7.5 µM ○; 11 µM ▲; 15 µM ▽. Dependence of main kinetic parameters K_m (B) and V_{max} (C) from the concentration of compound **RE-04**, the concentrations of inhibitor used were: 0, 7.5, 11 and 15 µM. All assays were performed by triplicate. The data reported in the graph, represent the means (A) or values (B and C) ± S.E.M.

2.4. Molecular docking of triterpene acids derivatives with PTP–1B

In order to gain insight into the putative binding mode of **RE-01**, **RE-02**, **RE-03** and **RE-04** with PTP–1B, these compounds were docked with a crystallographic structure of human PTP–1B. The crystallographic structure was obtained from the Protein Data Bank (PDB), accession code 1C83 [20]. This is the first study describing the docking of these triterpene derivatives with PTP–1B.

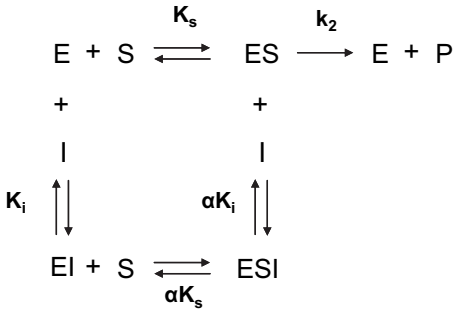

Scheme 1. The linear mixed-type inhibition of evaluated compounds. When the parameter $\alpha = 1$, the model describes the classical non-competitive inhibition.

Table 3
Values of the inhibition constants (*Ki*) and docking scores. The data shown represents the mean *Ki* values ± S.E.M.

Compound	*Ki* (µM)	α	Inhibition type	Docking score (kcal/mol)
RE-01	3.4 ± 0.7	3.4	Linear mixed type inhibition	−7.15
RE-02	6.0 ± 1.9	2.2	Linear mixed type inhibition	−7.59
RE-03	8.0 ± 2.0	2.3	Linear mixed type inhibition	−7.50
RE-04	7.1 ± 2.3	–	Non-competitive inhibition	−6.04

In addition to the PTP–1B catalytic site, Puius et al. identified a second aryl phosphate binding site in PTP–1B [21]. Fig. 9 shows the catalytic binding site (site A) and the second binding site (site B), as proposed by Puius et al. [21]. The most important residues of site B are Arg24, Arg254, and Glu262. Other residues in this site are Tyr46, Asp48, Val49, Ile219, and Met258 [21].

Before docking the triterpenic acids, the docking protocol was validated by predicting the binding mode of the crystallographic

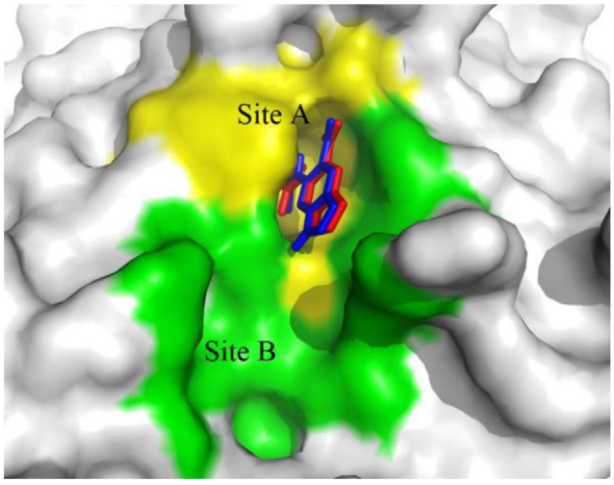

Fig. 9. Surface representation of the binding sites of PTP–1B. Catalytic binding site or site A, is shown in yellow; binding site B, as reported by Yoram et al. [21] is in green. A comparison between the binding position of the co-crystal ligand (red) and the binding position predicted by AutoDock (blue) is also shown. (For interpretation of the references to colour in this figure legend, the reader is referred to the web version of this article).

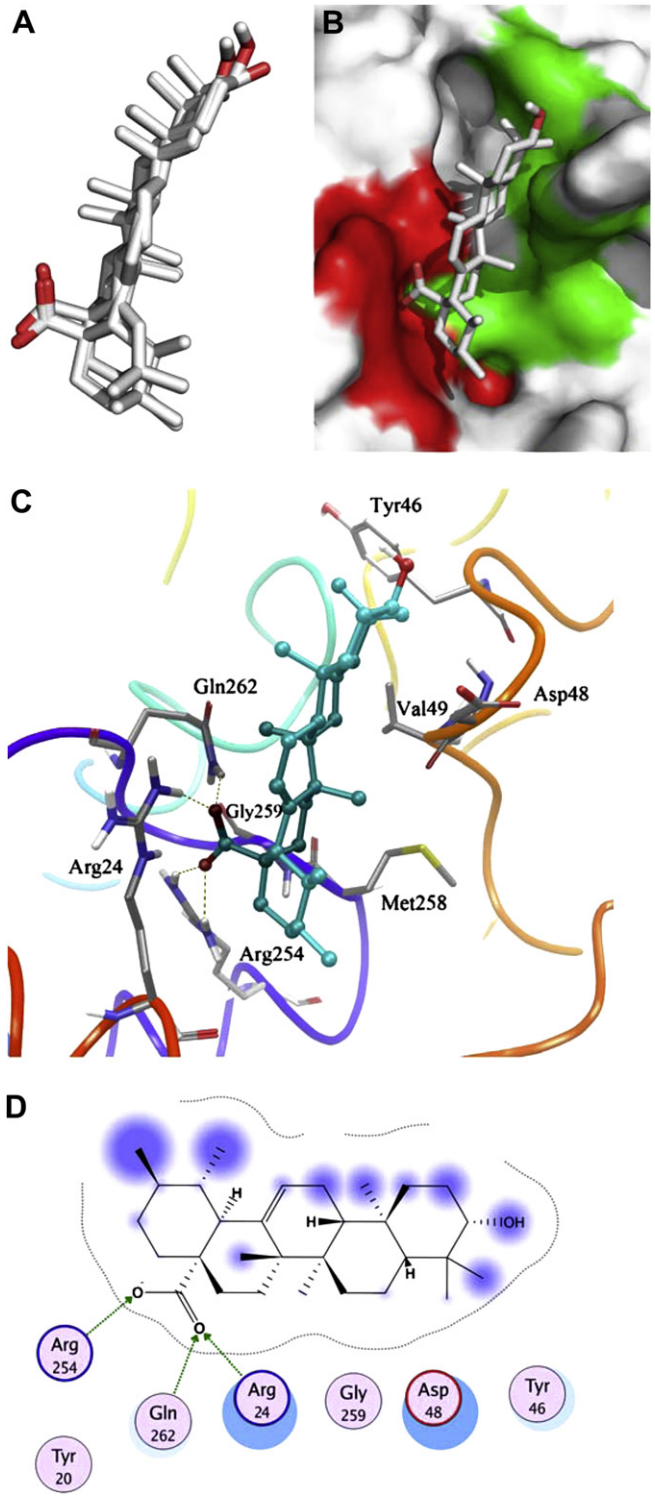

Fig. 10. Docking of triterpenic acids with PTP−1B. A) Overlay of all triterpenic binding modes. B) Surface representation of PTB−1B showing the binding mode of **RE-01** into the binding site B; residues forming hydrogen bonds with **RE-01** are shown in red. Residues making Van der Waals contacts with the ligand are shown in green. Figure generated with PyMOL 1.0 [24]. C) Three-dimensional binding model of **RE-01**. Hydrogen bonds are indicated with yellow dashes. D) Two-dimensional interaction diagram of the predicted binding mode of **RE-01**. The binding site residues are represented as follows: polar residues in pink, acidic residues with a red contour ring, basic residues with a blue contour ring. Green arrows indicate hydrogen bonding to side chain atoms, respectively. The ligand proximity contour is depicted with a dotted line. The ligand solvent exposure is represented with blue circles; larger and darker circles on ligand atoms indicate more solvent exposure. The receptor solvent exposure differences—in the presence and absence of the ligand—are represented by the size and intensity of the turquoise discs surrounding the residues; larger and darker discs indicate residues highly exposed to solvent in the active site when the ligand is absent. (For interpretation of the references to colour in this figure legend, the reader is referred to the web version of this article).

6-(oxalyl-amino)-1*H*-indole-5-carboxilic acid, a competitive inhibitor of PTP−1B [20]. Fig. 9 shows a comparison between binding mode of the crystallographic ligand and the binding mode predicted by AutoDock. Fig. 9 clearly shows that AutoDock successfully predicted the binding mode of crystallographic ligand with a root-mean square (RMS) deviation of 0.35 Å. Predicted binding energies for the triterpenes are summarized in Table 3. The four compounds showed comparable energies as calculated by AutoDock. Fig. 10 summarizes the binding modes of the triterpenic acids predicted by AutoDock. According to the docking models, all four compounds were predicted to bind into the site B, thus sharing a very similar binding mode (Fig. 10A and B). Interestingly, no binding poses were found by AutoDock into the catalytic binding site. Fig. 10C depicts the optimized binding mode of **RE-01**, the most active triterpene. In this binding model, the carboxylic group of **RE-01** at C28 forms an extensive hydrogen bond network with Arg24, Arg254 and Gln262; the surface of these residues is showed in red in Fig. 10B. Other residues that form van der Waals contacts with the triterpene are Tyr46, Asp48, Val49, Met258, and Gly259 (showed in green in Fig. 10B). Fig. 10D shows the corresponding two-dimensional interaction diagram of the optimized binding model generated with the program Molecular Operating Environment (MOE) [22].

3. Conclusions

We obtained four pentacyclic triterpenic acids from *P. reichenbachianum* with significant *in vivo* antidiabetic activity on non-insulin dependent diabetic rat model. Moreover, the main mode of action of triterpenic acids was produced by PTP−1B enzymatic inhibition with potent, reversible, selective, and linear mixed-type inhibition model. According to the docking results, the proposed binding mode of the triterpene derivatives in a second binding site (site B) of PTP−1B suggests a new strategy to obtain compounds with higher affinity and specificity. Arg254 and Gln262 are conserved among all PTPases, though other residues such as Gln262, Met258 and Gly259 are less conserved. Finally, pentacyclic triterpenic acids could be potential drugs for the treatment of type 2 diabetes as insulin sensitizer [23].

4. Experimental

4.1. Chemistry

Glibenclamide, nicotinamide, streptozotocin (STZ) and glucose (GLU) were purchased from Sigma−Aldrich Co. (St. Louis, MO, USA). Pentobarbital (Anestesal®) was obtained from Smith Kline Co. (Mexico City, Mexico). Test evaluations for GLU were acquired from Roche (ACCUTREND) (Mexico City, Mexico). Ursolic (RE-01), Oleanolic (RE-02), Moronic (RE-03) and Morolic (RE-04) acids were purified and characterized from acetone extract of leaves and stems of *P. reichenbachianum* (AEPr) as previously reported in Reference [10].

4.2. Biological assays

4.2.1. Expression and purification of recombinant PTPases

All experiments were performed using recombinant enzymes. Human PTP−1B, the IF1 and IF2 isoenzymes of LMW-PTP, and the yeast LMW-PTP (LTP1) were prepared and purified in our laboratory, whereas the recombinant catalytic domain of LAR (Leukocyte

antigen-related PTPase) was purchased from Sigma. Recombinant enzymes were expressed in a bacterial line and purified by chromatography techniques. Briefly, the complete sequence of PTP–1B, IF1, IF2, and LTP1 were cloned in the pGEX–2T bacterial expression vector downstream the GST sequence. These vectors were used to transform *Escherichia coli* TB1 strain. The recombinant fusion proteins were purified from bacterial lysate using a single-step affinity chromatography on glutathione-agarose. The solution containing each purified fusion protein was treated with thrombin for 3 h at 37 °C. Then the active PTPases were purified from GST and thrombin by gel filtration on a Superdex G75 column. The purity of all enzymes was assessed by SDS–PAGE.

4.2.2. Enzyme assays

All assays were carried out at 37 °C. The substrate (*p*NPP) was dissolved in 0.075 M of β,β-dimethylglutarate buffer pH 7.0, containing 1 mM EDTA and 1 mM dithiothreitol. The final volume was 1 ml. The reactions were initiated by adding appropriate aliquots of the enzyme, and stopped at final times with 4 ml of 1 M KOH. The released *p*-nitrophenolate ion was determined by reading the absorbance at 400 nm ($\epsilon = 18{,}000\ M^{-1}\ cm^{-1}$). The main kinetic parameters (K_m and V_{max}) were determined by measuring the initial rates using eight different substrate concentrations in the 0.5–40 mM range. Experimental data was analyzed using the Michaelis equation and a nonlinear fitting program (FigSys).

4.2.3. Animals

Male Wistar rats weighing 200–250 g body weight were housed at standard laboratory conditions and fed with a rodent pellet diet and water *ad libitum*. They were maintained at room temperature and a photoperiod of 12 h day/night cycle. Animals described as fasted were deprived of food for 16 h but had free access to water. All animal procedures were conducted in accordance with our Federal Regulations for Animal Experimentation and Care (SAGARPA, NOM-062-ZOO-1999, México), and approved by the Institutional Animal Care and Use Committee based on US National Institute for Health publication (No. 85–23, revised 1985).

4.2.4. Induction of diabetes

Streptozotocin (STZ) was dissolved in citrate buffer (pH 4.5) and nicotinamide was dissolved in normal physiological saline solution. T2DM was induced in overnight fasted rats by a single intraperitoneal injection of 65 mg/kg streptozotocin, 15 min after the i.p. administration of 110 mg/kg of nicotinamide. Hyperglycemia was confirmed by the elevated glucose concentration in plasma, determined at 72 h by glucometer. The animals with blood glucose concentration higher 250 mg/dl were used for the antidiabetic screening.

4.2.5. In vivo antidiabetic assay (T2DM model)

The diabetic animals were divided into groups of six animals each ($n = 6$). Rats of experimental groups were orally administered a suspension of the compounds (prepared in 10% Tween 80) (50 mg/kg body weight) and a similar suspension of dry acetone extract (100 mg/kg body weight). Control group animals were also fed with 10% Tween 80. Glibenclamide (5 mg/kg) was used as hypoglycemic reference drug. Blood samples were collected from the caudal vein at 0, 1, 3, 5 and 7 h after vehicle, sample and drug administration. Blood glucose concentration was estimated by enzymatic glucose oxidase method using a commercial glucometer (Accutrend GCT, Roche®). The percentage variation of glycemia for each group was calculated in relation to initial (0 h) level, according to: %Variation of glycemia $= [(G_x - G_0)/G_0] \times 100$, where G_0 were initial glycemia values and G_x were the glycemia values at +1, +3, +5 and +7 h respectively. All values were expressed as mean ± S.E.M. Statistical significance was estimated by analysis of variance (ANOVA), $p < 0.05$ and $p < 0.01$ implies significance.

4.3. Docking

Molecular Operating Environment (MOE) 2009.10 was used for ligand and protein preparation, and molecular structure viewing. The crystal structure was obtained from the PDB with the accession code 1C83 [20]. Docking calculations were conducted with AutoDock, version 4.0 [24] In short, AutoDock performs an automated docking of the ligand with user-specified dihedral flexibility within a protein rigid binding site. The program performs several runs in each docking experiment. Each run provides one predicted binding mode. All water molecules and 6-(oxalyl-amino)-1*H*-indole-5-carboxilic acid (crystallographic ligand) were removed from the crystallographic structure and all hydrogen atoms were added. For all ligands and protein, Gasteiger charges were assigned and nonpolar hydrogen atoms were merged. All torsions were allowed to rotate during docking. The auxiliary program AutoGrid generated the grid maps. Each grid was centered at the crystallographic coordinates of the crystallographic compound. The grid dimensions were 22.12 × 22.12 × 22.12 $Å^3$ with points separated by 0.375 Å. Lennard–Jones parameters 12–10 and 12–6, supplied with the program, were used for modeling H-bonds and Van der Waals interactions, respectively. The Lamarckian genetic algorithm was applied for the search using default parameters. The number of docking runs was 100. After docking, the 100 solutions were clustered into groups with RMS lower than 1.0 Å. The clusters were ranked by the lowest energy representative of each cluster. In order to describe the ligand-binding pocket interactions, the top ranked binding mode found by AutoDock in complex with the binding pocket of PTP–1B was subject to full energy minimization using the MMFF94 force field implemented in MOE until the gradient 0.05 was reached. PyMOL 1.0 [25] was used to generate the molecular surface of docking models.

Acknowledgments

This study was financed by a grant from Fondo de Consolidación-UAEM (Apoyo a Cuerpos Académicos 2009), and Faculty of Pharmacy budgets (2009 and 2010). J. J. Ramírez-Espinosa is grateful to CONACyT for the scholarship grants (349728). F. Lopez-Vallejo and JL. Medina-Franco thank the State of Florida, Executive Office of the Governor's Office of Tourism, Trade, and Economic Development. P. Paoli and G. Camici thank the Ente Cassa di Risparmio di Firenze for financial support. Authors are very grateful to Kyle Kryak (TPIMS) for proofreading the manuscript.

Appendix. Supplementary material

Supplementary data related to this article can be found online at doi:10.1016/j.ejmech.2011.03.005.

References

[1] WHO Fact sheet #312 November 2009 [on line July 22th 2010], http://www.who.int/mediacentre/factsheets/fs312/en/index.html.
[2] T.M. Hung, D.M. Hoang, J.C. Kim, J.S. Ahn, B.S. Min, Protein tyrosine phosphatase 1B inhibitory by dammaranes from Vietnamese Giao-Co-Lam tea, J. Ethnopharmacol. 124 (2009) 240–245.
[3] S.M. Grundy, Drug therapy of the metabolic syndrome: minimizing the emerging crisis in polypharmacy, Nat. Rev. Drug Discov. 5 (2006) 295–309.
[4] K.B. Sotiropoulos, A. Clermont, Y. Yasuda, C. Rask-Madsen, M. Matsumoto, J. Takahashi, K. Della Vecchia, T. Kondo, L.P. Aiello, G.L. King, Adipose-specific effect of rosiglitazone on vascular permeability and protein kinase C activation: novel mechanism for PPARγ agonist's effects on edema and weight gain, FASEB J. 20 (2006) 1203–1205.

[5] A.J. Scheen, L.F. Van Gaal, Sitagliptine (Januvia): incretin enhancer potentiating insulin secretion for the treatment of type 2 diabetes, Rev. Med. Liege 63 (2008) 105–109.
[6] T.O. Johnson, J. Ermolieff, M.R. Jirousek, Protein tyrosine phosphatase 1B inhibitors for diabetes, Nat. Rev. Drug Discov. 1 (2002) 696–709.
[7] Y. Romsicki, M. Reece, J.Y. Gauthier, E. Asante-Appiah, B.P. Kennedy, Protein tyrosine phosphatase dephosphorylation of the insulin receptor occurs in a perinuclear endosome compartment in human embryonic kidney 293 cells, J. Biol. Chem. 279 (2004) 12868–12875.
[8] M. Elchebly, P. Payette, E. Michaliszyn, W. Cromlish, S. Collins, A.L. Loy, D. Normandin, A. Cheng, J. Himms-Hagen, C.C. Chan, C. Ramachandran, M.J. Gresser, M.L. Tremblay, B.P. Kennedy, Increased insulin sensitivity and obesity resistance in mice lacking the protein tyrosine phosphatase gene, Science 283 (1999) 1544–1548.
[9] A. Andrade-Cetto, M. Heinrich, Mexican plants with hypoglycaemic effect used in the treatment of diabetes, J. Ethnophamacol. 99 (2005) 325–348.
[10] M.Y. Rios, D. Salinas, M.L. Villareal, Cytotoxic activity of moronic acid and identification of the new triterpene 3,4-seco-olean-18-ene-3,28-dioic acid from *Phoradendron reichenbachianum*, Planta Med. 67 (2000) 443–446.
[11] M. Kurokawa, P. Basnet, M. Ohsugi, T. Hozumi, S. Kadota, T. Namba, T. Kawana, K. Shiraki, Anti-herpes simplex virus activity of moronic acid purified from *Rhus javanica* in vitro and in vivo, J. Pharmacol. Exp. Ther. 289 (1999) 72–78.
[12] S.M. Jang, M.J. Kim, M.S. Choi, E.Y. Kwon, M.K. Lee, Inhibitory effects of ursolic acid on hepatic polyol pathway and glucose production in streptozotocin-induced diabetic mice, Metabolism 59 (2010) 512–519.
[13] R.M. Perez Gutierrez, R. Vargas Solis, E. Garcia Baez, E. Gallardo Navarro, Hypoglycemic activity of constituents from *Astianthus viminalis* in normal and strptozotocin-induced diabetic mice, J. Nat. Med. 63 (2009) 393–401.
[14] C.L. De Melo, M.G.R. Queiroz, S.G.C. Fonseca, A.M.C. Bizerra, T.L.G. Lemos, T.S. Melo, F.A. Santos, V.S. Rao, Oleanolic acid, a natural triterpenoid improves blood glucose tolerance in normal mice and ameliorates visceral obesity in mice fed a high-fat diet, Chem. Biol. Interact. 185 (2010) 59–65.
[15] W. Zhang, D. Hong, Y. Zhou, Y. Zhang, Q. Shen, J.Y. Li, L.H. Hu, J. Li, Ursolic acid and its derivative inhibit protein tyrosine phosphatase 1B, enhancing insulin receptor phosphorylation and stimulating glucose uptake, Biochim. Biophys. Acta 1760 (2006) 1505–1512.
[16] Y.N. Zhang, W. Zhang, D. Hong, L. Shi, Q. Shen, J.Y. Li, J. Li, L.H. Hu, Oleanolic acid and its derivatives: new inhibitor of protein tyrosine phosphatase 1B with cellular activities, Bioorg. Med. Chem. 16 (2008) 8697–8705.
[17] A. Blum, A.D. Favia, E. Maser, 11beta-Hydroxysteroid dehydrogenase type 1 inhibitors with oleanan and ursan scaffolds, Mol. Cell. Endocrinol. 301 (2009) 132–136.
[18] J.M. Rollinger, D.V. Kratschmar, D. Schuster, P.H. Pfisterer, C. Gumy, E.M. Aubry, S. Brandstötter, H. Stuppner, G. Wolber, A. Odermatt, 11beta-Hydroxysteroid dehydrogenase 1 inhibiting constituents from *Eriobotrya japonica* revealed by bioactivity-guided isolation and computational approaches, Bioorg. Med. Chem. 18 (2010) 1507–1515.
[19] S.H. Jung, Y.J. Ha, E.K. Shim, S.Y. Choi, J.L. Jin, H.S. Yun-Choi, J.R. Lee, Insulin-mimetic and insulin-sensitizing activities of a pentacyclic triterpenoid insulin receptor activator, Biochem. J. 403 (2007) 243–250.
[20] H.S. Andersen, L.F. Iversen, C.B. Jeppesen, S. Branner, K. Norris, H.B. Rasmussen, K.B. Møller, N.P. Møller, 2-(oxalylamino)-benzoic acid is a general, competitive inhibitor of protein-tyrosine phosphatases, J. Biol. Chem. 275 (2000) 7101–7108.
[21] Y.A. Puius, Y. Zhao, M. Sullivan, D.S. Lawrence, S.C. Almo, Z.-Y. Zhang, Identification of a second aryl phosphate-binding site in protein-tyrosine phosphatase 1b: a paradigm for inhibitor design, Proc. Natl. Acad. Sci. U.S.A. 94 (1997) 13420–13425.
[22] Molecular Operating Environment (MOE), Version 2009.10, Chemical Computing Group Inc., Montreal, Quebec, Canada. Available at: http://www.chemcomp.com.
[23] R. Sarabu, J. Tilley, Recent advances in therapeutic approaches to type 2 diabetes. in: A.M. Doherty (Ed.), Annual Reports in Medicinal Chemistry, vol. 40. Elsevier: Academic Press, 2005, pp. 167–181.
[24] R. Huey, G.M. Morris, A.J. Olson, D.S. Goodsell, A semiempirical free energy force field with charge-based desolvation, J. Comput. Chem. 28 (2007) 1145–1152.
[25] W.L. DeLano "The PyMOL Molecular Graphics System." DeLano Scientific LLC, San Carlos, CA, USA. Available at: http://www.pymol.org.